

In situ growth of layered double hydroxides on boehmite AlOOH for the active and stable oxygen evolution in alkaline media

Shijie He^a, Hua Lin^{*ab}

^a School of Materials and Energy, Southwest University, Chongqing, 400715, P. R. China. E-mail: lh2004@swu.edu.cn

^b Chongqing Key Laboratory for Advanced Materials and Technologies of Clean Energies, Chongqing 400715, P. R. China.

Experimental

Materials and Synthesis.

Synthesis of pure and metal-doped boehmite γ -AlOOH (referred simply as AlOOH in the following text) nanorods. The AlOOH nanorods were prepared through a one-pot, and surfactant-free hydrothermal method. Typically, 2 mmol of $\text{AlCl}_3 \cdot 6\text{H}_2\text{O}$ (AR, Aladdin) powders were dissolved in 70 mL of deionized water by stirring and ultrasonication, followed by the addition of 6 mL of formamide (AR, Aladdin). The pH was measured to be about 6.22. After fully stirring, the as-prepared solution was sealed inside a Teflon-lined autoclave, kept at 220 °C for 24 h. And then, the autoclave was cooled down in air. Finally, the precipitation was sequentially centrifuged with ethanol and deionized water for several times, and then frozen dried. The V-doped AlOOH nanorods were synthesized through the same procedure, except for the addition of V_2O_5 (0.25 mmol, AR, Aladdin) into the original reaction system. As for the Ni-doped AlOOH nanorods, besides the addition of $\text{NiCl}_2 \cdot 6\text{H}_2\text{O}$ (0.5 mmol, AR, Aladdin), 8 mmol of $\text{C}_2\text{H}_2\text{O}_4 \cdot 2\text{H}_2\text{O}$ was also added to provide a more moderate situation in case of the reduction of Ni^{2+} to be elementary Ni.

Synthesis of FeCo and FeNi layered double hydroxides (LDH). Regarding on the FeCo layered double hydroxides, to synthesize the Fe_1Co_1 (whereas the subscripts only stand for the molar ratio of Fe and Co in the as-prepared products, but not mean that they form a sole compound) LDH ultrathin films, 0.5 mmol of $\text{Fe}(\text{NO}_3)_3 \cdot 9\text{H}_2\text{O}$ (AR, Aladdin) powders and 0.5 mmol of $\text{Co}(\text{NO}_3)_2 \cdot 6\text{H}_2\text{O}$ (AR, Aladdin) powders were dissolved in 20 mL of deionized water heated at 80 °C, immediately followed by the addition of 0.4 g NaOH and 20 mL of formamide aqueous solution (containing 4.6 mL of formamide) which was already at 80 °C. The pH was measured to be about 12.95. The mixture was kept at 80 °C for 10 min and then cooled down in air. Finally, the precipitation was centrifuged with a mixture of ethanol and deionized water (at a volume ratio of 1:1) for several times, and then frozen dried. As for the Fe_3Co_1 and Fe_1Co_3 LDH, the synthetic procedures are the same except for the amount of metal sources (0.75 mmol of $\text{Fe}(\text{NO}_3)_3 \cdot 9\text{H}_2\text{O}$ and 0.25 mmol of $\text{Co}(\text{NO}_3)_2 \cdot 6\text{H}_2\text{O}$ for Fe_3Co_1 , while 0.25 mmol of $\text{Fe}(\text{NO}_3)_3 \cdot 9\text{H}_2\text{O}$ and 0.75 mmol of $\text{Co}(\text{NO}_3)_2 \cdot 6\text{H}_2\text{O}$ for Fe_1Co_3). The synthesis of FeNi LDH followed the same strategy as that of FeCo LDH while the Ni source was $\text{Ni}(\text{NO}_3)_2 \cdot 6\text{H}_2\text{O}$ (AR, Aladdin).

Synthesis of pure or metal-doped AlOOH supported layered double hydroxides. Taking the synthesis of AlOOH/FeCo-LDH as an example, 0.06 g of as-synthesized AlOOH nanorods were fully dissolved by stirring and ultrasonication in 20 mL of deionized water. Then the solution was heated to 80 °C. Immediately, 0.5 mmol of $\text{Fe}(\text{NO}_3)_3 \cdot 9\text{H}_2\text{O}$ powders and 0.5 mmol of $\text{Co}(\text{NO}_3)_2 \cdot 6\text{H}_2\text{O}$ powders were dissolved in the solution, followed by the addition of 0.4 g of NaOH and 20 mL of formamide aqueous solution (containing 4.6 mL of formamide) which was already at 80 °C. The mixture was then kept at 80 °C for 10 min and then cooled down in air. Finally, the precipitation was centrifuged with a mixture of ethanol and deionized water (at a

volume ratio of 1:1) for several times, and then frozen dried. The synthesis of other metal-doped AlOOH supported LDH followed the same strategy. Note that the amount of metal-doped AlOOH was always 0.06 g, and the molar ratio of the metals in the LDH films were always 1:1.

Characterizations.

HRTEM images were collected by using JEOL JEM-2100F high-resolution transmission electron microscope operating at 120 kV and 300 kV, respectively. And the samples for HRTEM investigations were prepared by slightly stirring the copper grid in a dilute dispersion containing the desired sample, leaving the solvent to evaporate at room temperature. XRD patterns were recorded by a Shimadzu XRD-6100 X-ray diffractometer with Cu K α irradiation ($\lambda = 0.15406$ nm) operated at 40 kV and 30 mA in the 2θ scan range of 5-80° at a scan rate of 5 deg min⁻¹. FESEM images and EDS maps were obtained on a JSM-7800F field emission scanning electron microscope equipped with an energy-dispersive X-ray spectrometer operated at 15 kV. X-ray photoelectron spectroscopy measurements were carried out on a Thermo Scientific Escalab 250Xi spectrometer at 2×10^{-10} mbar with a monochromatic Al K α radiation ($E = 1486.6$ eV). BET equation based on the nitrogen adsorption isotherm obtained with a Micromeritics Gemini VII apparatus (Surface Area and Porosity System) under vacuum at 250 °C for 4 h prior to the measurements and the pore size distribution was determined with the BJH method applied to the desorption branch of the adsorption-desorption isotherm. The UV-vis absorption spectra were measured on a Hitachi U-3310 UV-vis spectrophotometer by analyzing 3.5 mL of deionized water dissolved with 0.3 mg of the as-prepared samples.

Electrochemical Tests.

Electrode preparation. The concentration of catalyst suspension was determined by drying a portion of suspension and weighing the dry powder. To obtain the catalyst ink, 5 mg of the desired sample, 0.5 wt% Nafion solution (10 μ L) was added into a solution (990 μ L) containing ethanol and deionized water (1:1, in volume ratio) by ultrasonication in a water bath for 10 min. Then 11 μ L of the catalyst ink was dropped on the surface of a glassy carbon ring-disk rotating disk electrode (RRDE, diameter: 5 mm, area: 0.196 cm²) which was dried in air to evaporate solvent. The final catalyst loading was about 0.28 mg cm⁻². The RRDE electrode was polished using aqueous alumina suspension on felt polishing pads before the use.

Oxygen evolution reaction measurement. All the potentials written here are reported versus the reversible hydrogen electrode (RHE) at the working pH, unless otherwise stated. Pt wire and Ag/AgCl (3.5 M KCl) were used as counter and reference electrodes, respectively. And the potential difference between the working electrode and the Ag/AgCl reference electrode was converted to the RHE scale via the following Nernst equation:

$$E_{RHE} = E_{Ag/AgCl(sat.KCl)} + E_{Ag/AgCl(sat.KCl)}^0 + 0.0591 \times pH$$

Where E_{RHE} is the potential on the RHE scale, $E_{Ag/AgCl(sat. KCl)}$ is the potential applied experimentally, $E^0_{Ag/AgCl(sat. KCl)}$ is the standard potential of the Ag/AgCl redox couple in a solution saturated with KCl on the normal hydrogen electrode scale (0.197 V), and pH is the very pH of the working electrolyte (1 M KOH, pH = 13.6). All the polarization curves from all catalysts were iR -corrected, in which i is the measured working electrode current and the R is the series resistance that arises from the working electrode substrate and electrolyte resistances. And R was determined by the high frequency intercept from the Nyquist plot obtained by the electrochemical impedance spectroscopy (EIS) technique. EIS measurements were performed by applying an AC voltage with 5 mV amplitude in a frequency range from 100000 to 0.1 Hz and recorded at the open circuit potentials. In O₂-saturated 1.0 M KOH electrolyte, the value of R typically ranges from 5 to 10 Ω . During all electrocatalytic measurements, the RDE continuously rotated at 1600 rpm to get rid of the oxygen bubbles. For the stability test, chronopotentiometry (CP) was carried out under a constant current density of 10 mA cm⁻² with the catalyst loaded RDE as the working electrode. For electrochemical data collection, linear sweep voltammetry (LSV) was carried out at 5 mV s⁻¹ for the polarization curves. The Tafel slope was calculated according to Tafel equation as follows:

$$\eta = b \log(j) + a$$

Where η denotes the overpotential, b denotes the Tafel slope, j denotes the current density, and a denotes the exchange current density. The overpotential was calculated as follows:

$$\eta = E(vs RHE) - 1.23$$

considering O₂/H₂O equilibrium at 1.23 V vs RHE.

Electrochemical active surface area (ECSA). The electrical double layer capacitance (C_{dl}) of the as-synthesized materials was measured from double-layer charging curves using cyclic voltammograms (CVs) in a small potential range of 1.2-1.3 V vs RHE. The working electrodes were scanned for several potential cycles until the signals were stabilized, and then the CV data were collected. The plot of the current density (at 1.25 V vs RHE) against scan rate has a linear relationship and its slope is the C_{dl} of the tested catalyst. The C_{dl} was used to stand for the ECSA of each catalyst.

Turnover frequency (TOF). The TOF values are calculated according to the equation:

$$TOF = \frac{J \times A}{4 \times F \times m}$$

Where J is the current density at a given overpotential (for example, $\eta = 254$ mV), A is the surface area of the electrode, F is the Faraday constant, and m is the number of moles of metal on the electrode. Since Al atoms don't show any electrocatalytic activities for the OER, all the other metal (Fe, Ni, Co and V) atoms are considered as the active sites and herein to be accessible for catalyzing the OER. As the doped metal (for example, Ni and V) atoms are normally regarded to substitute the host metal (for example, Al) sites in a unit cell, we assumed that the doped metal atoms take the coordination as MOOH (M = Ni, V) when calculating the moles of the deposited samples on the electrode. Regarding on the mixed-valence state of Fe, Co, and Ni atoms in LDHs, we treated the coordinations of LDHs as M(OH)_{2.5} (M = Fe, Ni, Co) as the

number of atoms of M(II) was almost equal to that of M(III), which was proved by the XPS data.

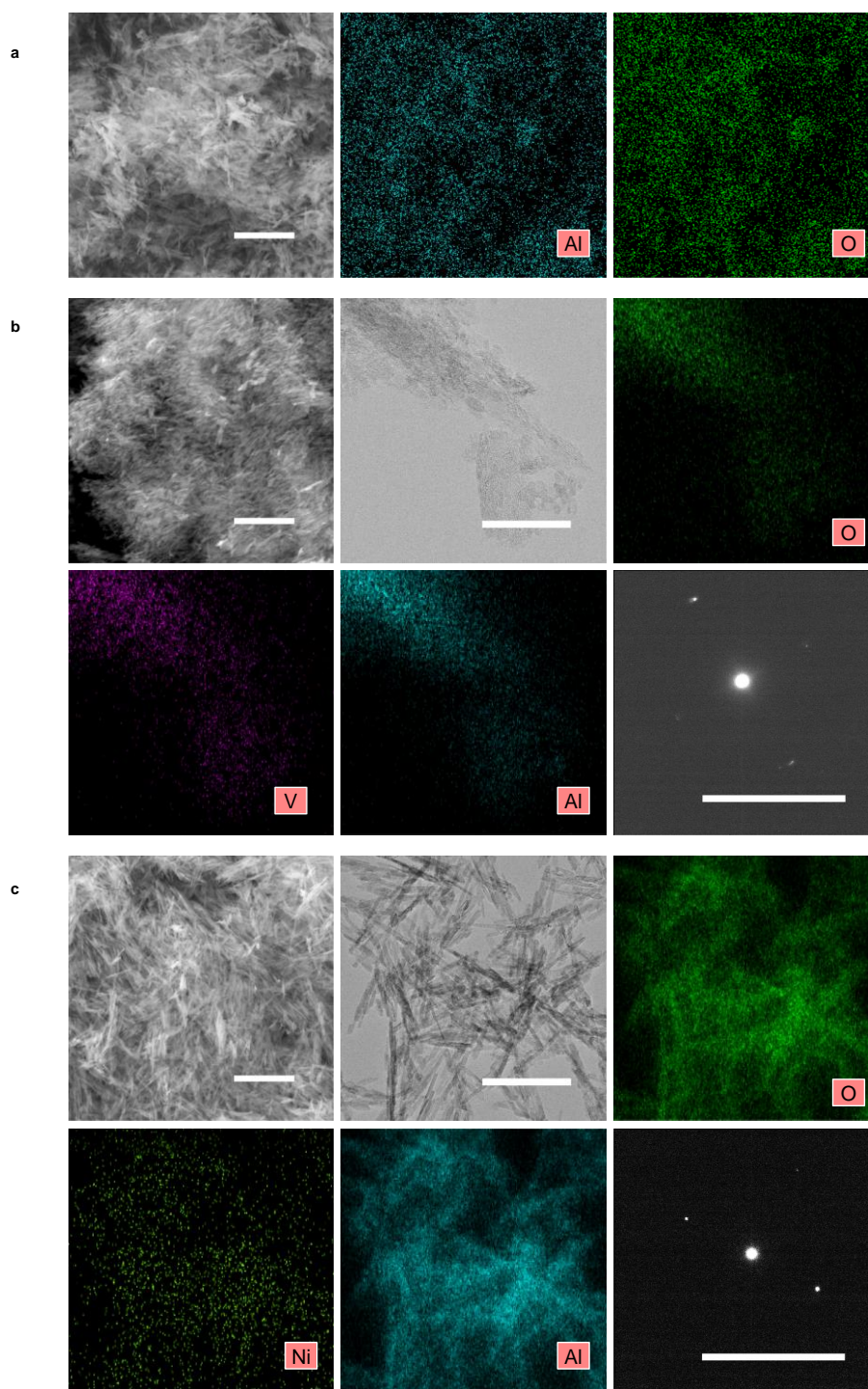


Fig. S1 Electron microscopy investigation of the nanorods. a) FESEM image and the corresponding EDS mappings of AlOOH nanorods. b) FESEM image, TEM image and the corresponding EDS mappings and SAED pattern of V-AlOOH nanorods. c) FESEM image, TEM image and the corresponding EDS mappings and SAED pattern of Ni-AlOOH nanorods. Scale bar: 1 μm for all the FESEM images, 200 nm for the TEM image in b) and 500 nm for the TEM image in c).

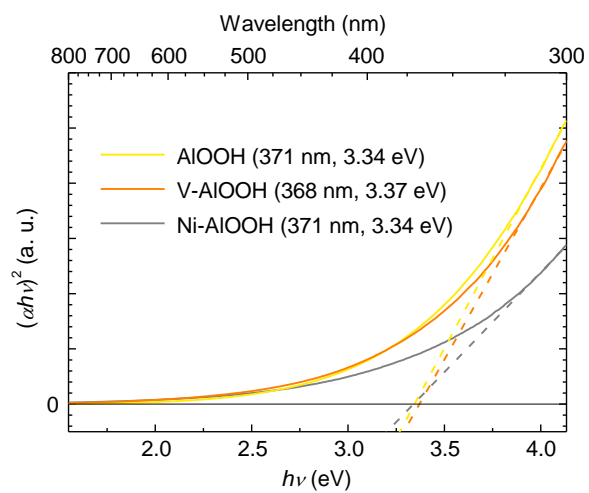


Fig. S2 Tauc plots of the pristine, V- and Ni-doped AlOOH nanorods.

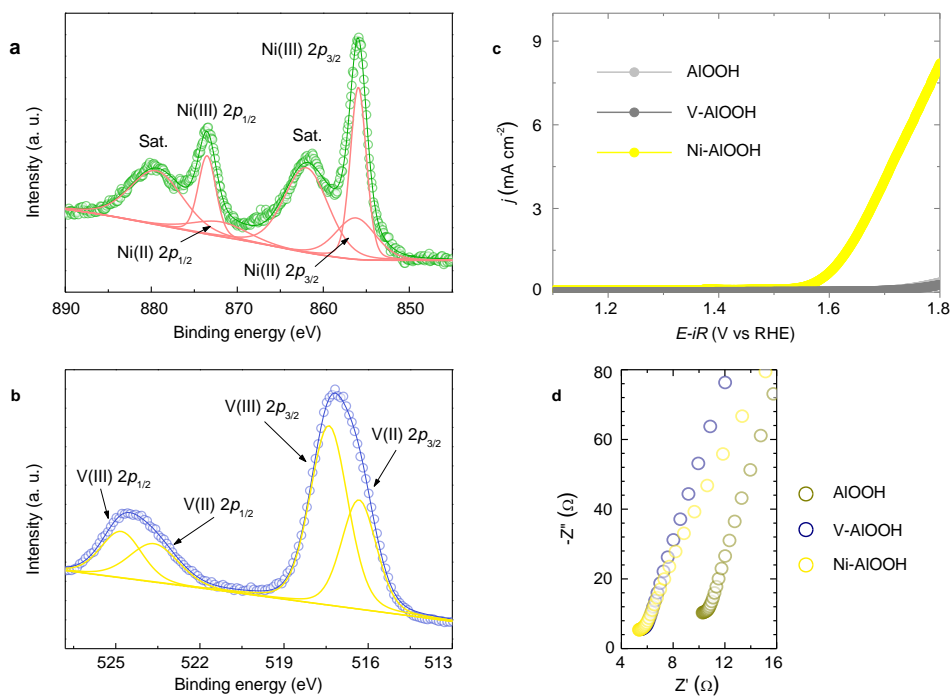


Fig. S3 a) Ni $2p$ XPS spectrum for Ni-AIOOH. b) V $2p$ XPS spectrum for V-AIOOH. c) LSV curves and d) Nyquist plots of the pristine, V- or Ni-doped AIOOH O₂-saturated 1 M KOH at 1600 rpm.

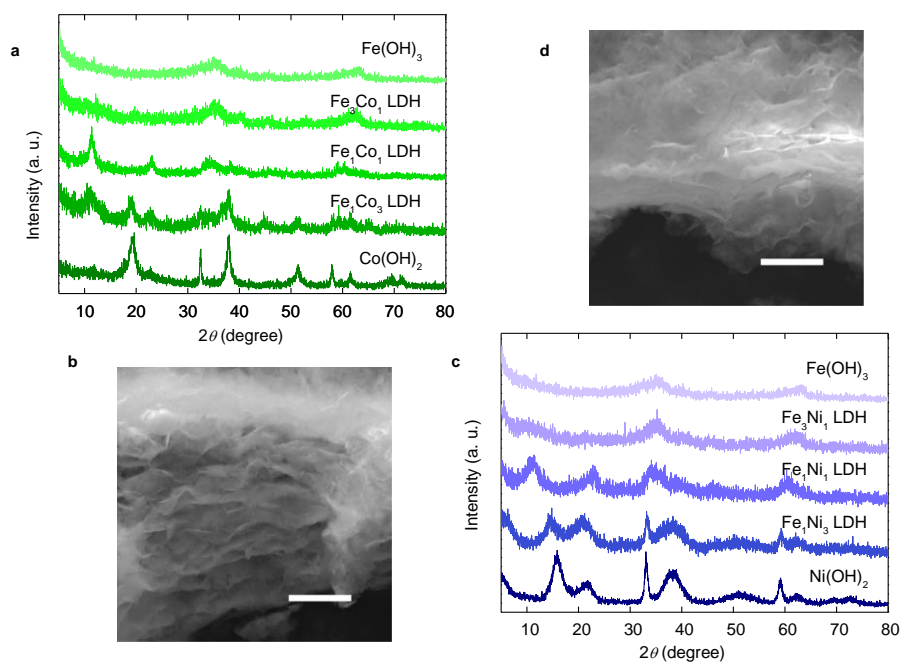


Fig. S4 XRD patterns of a) FeCo LDHs (the Fe contents of these five samples are gradually decreased associated with the sequence from the topmost to the bottom; the topmost pattern can be indexed to Fe(OH)₃ with standard PDF card No. 22-0346, while bottom to Co(OH)₂ with standard PDF card No. 30-0443) and c) FeNi LDHs (the Fe contents of these five samples are gradually decreased associated with the sequence from the topmost to the bottom; the bottom pattern can be indexed to Ni(OH)₂ with standard PDF card No. 14-0117, while the Fe₁Ni₁ LDH to FeNi LDH with standard PDF card No. 51-0463). FESEM images of b) Fe₁Co₁ LDH and d) Fe₁Ni₁ LDH. Scale bar: 1 μm for both b) and d).

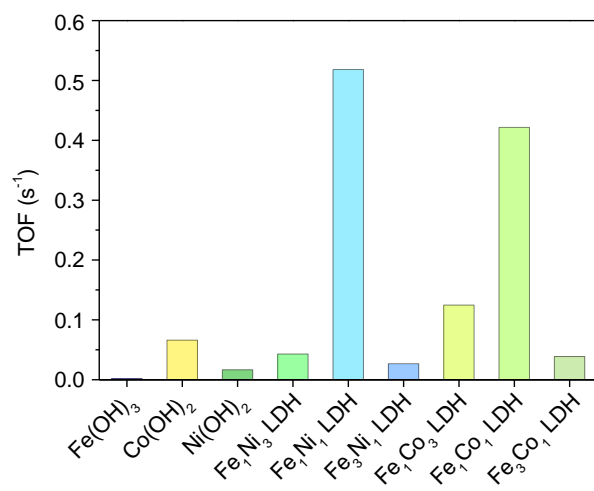


Fig. S5 TOFs of the LDHs calculated from the current at $\eta = 300$ mV.

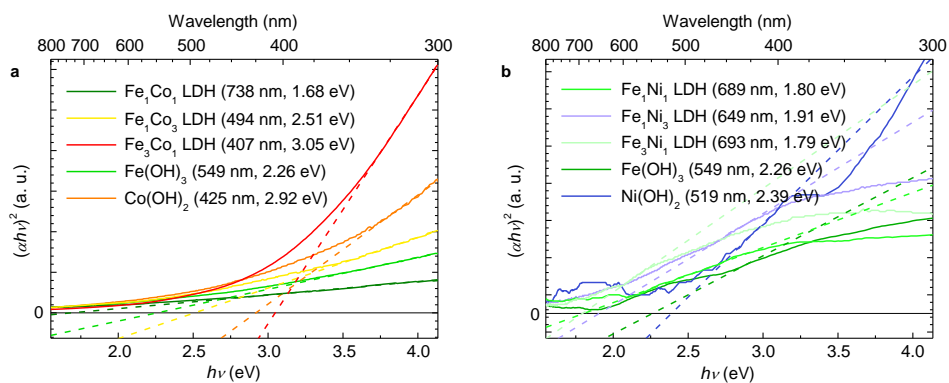


Fig. S6 Tauc plots of a) FeCo LDHs and b) FeNi LDHs. As for FeCo LDHs, the Fe_1Co_1 LDH obtains the narrowest band gap of about 1.68 eV which is much smaller than those of other FeCo LDHs, demonstrating that the electronic structure of FeCo LDHs are quite sensitive to the components. The band gaps of FeNi LDHs also decreased compared with the pristine $\text{Fe}(\text{OH})_3$ and $\text{Ni}(\text{OH})_2$, but the shifts are smaller.

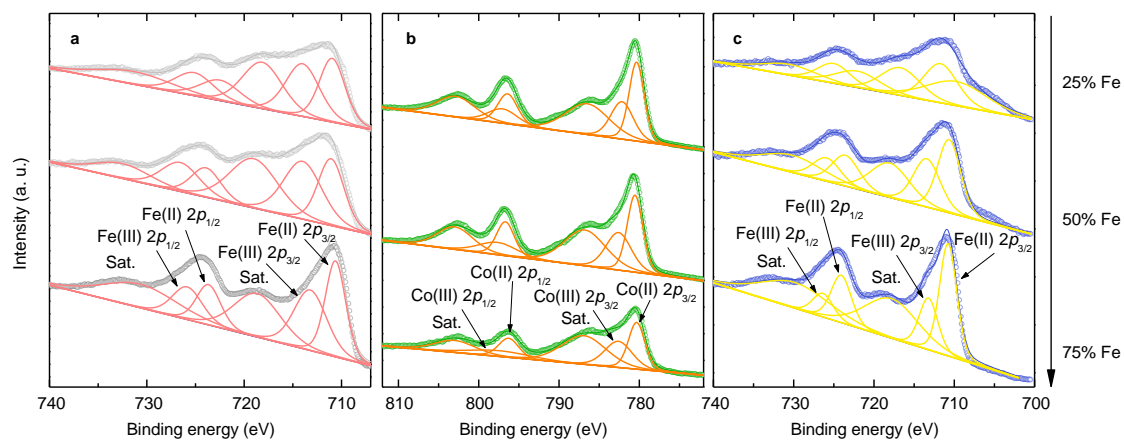


Fig. S7 a) Fe 2p XPS spectra for FeNi LDHs. b) Co 2p and c) Fe 2p XPS spectra for FeCo LDHs. The Fe contents of the three samples in each figure are gradually increased associated with the sequence from the topmost to the bottom.

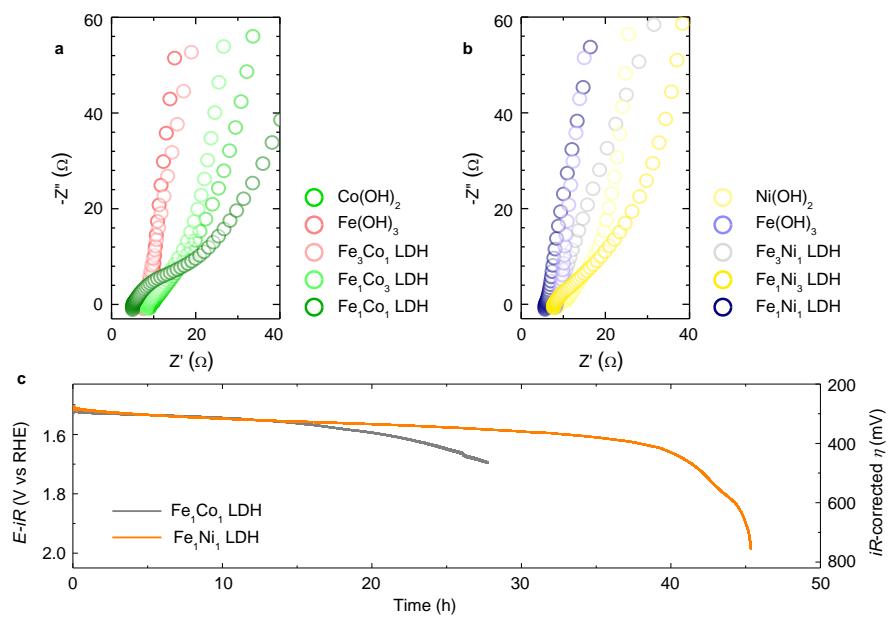


Fig. S8 Electrochemical measurements of LDHs. Nyquist plots of impedance for a) FeCo LDHs and b) FeNi LDHs O_2 -saturated 1 M KOH at 1600 rpm. c) CP measurements at 10 mA cm^{-2} for Fe_1Co_1 and Fe_1Ni_1 LDHs.

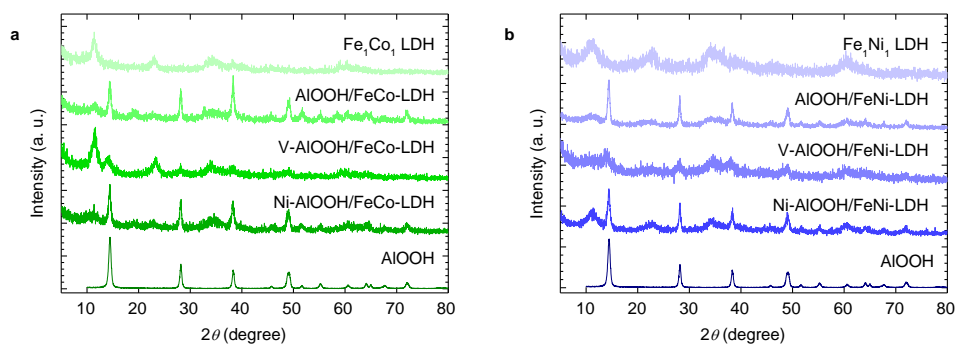


Fig. S9 XRD patterns of a) Fe₁Co₁-based composites and b) Fe₁Ni₁-based composites.

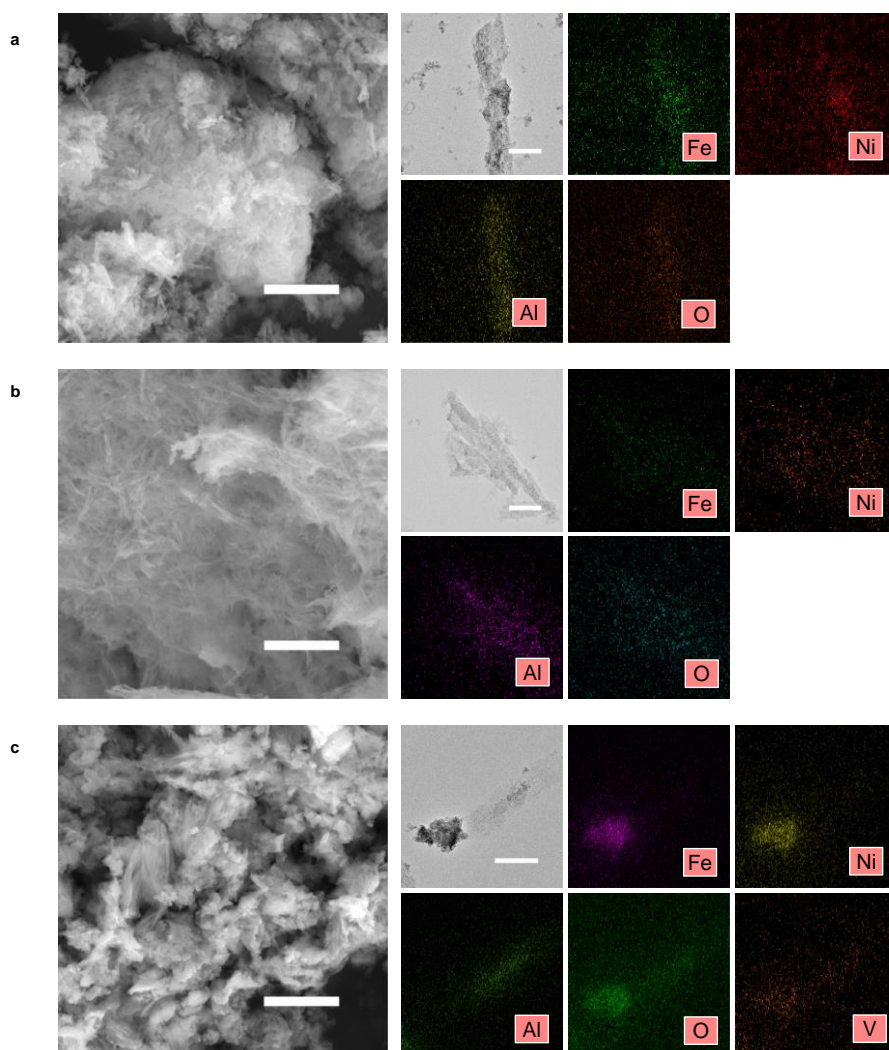


Fig. S10 Electron microscopy measurements for Fe₁Ni₁-LDH-based composites. FESEM images, TEM images and corresponding EDS mappings of a) AlOOH/FeNi-LDH, b) Ni-AlOOH/FeNi-LDH and c) V-AlOOH/FeNi-LDH. Scale bar in FESEM images: 1 μ m. Scale bar in TEM images: 100 nm for a) and b), 200 nm for c).

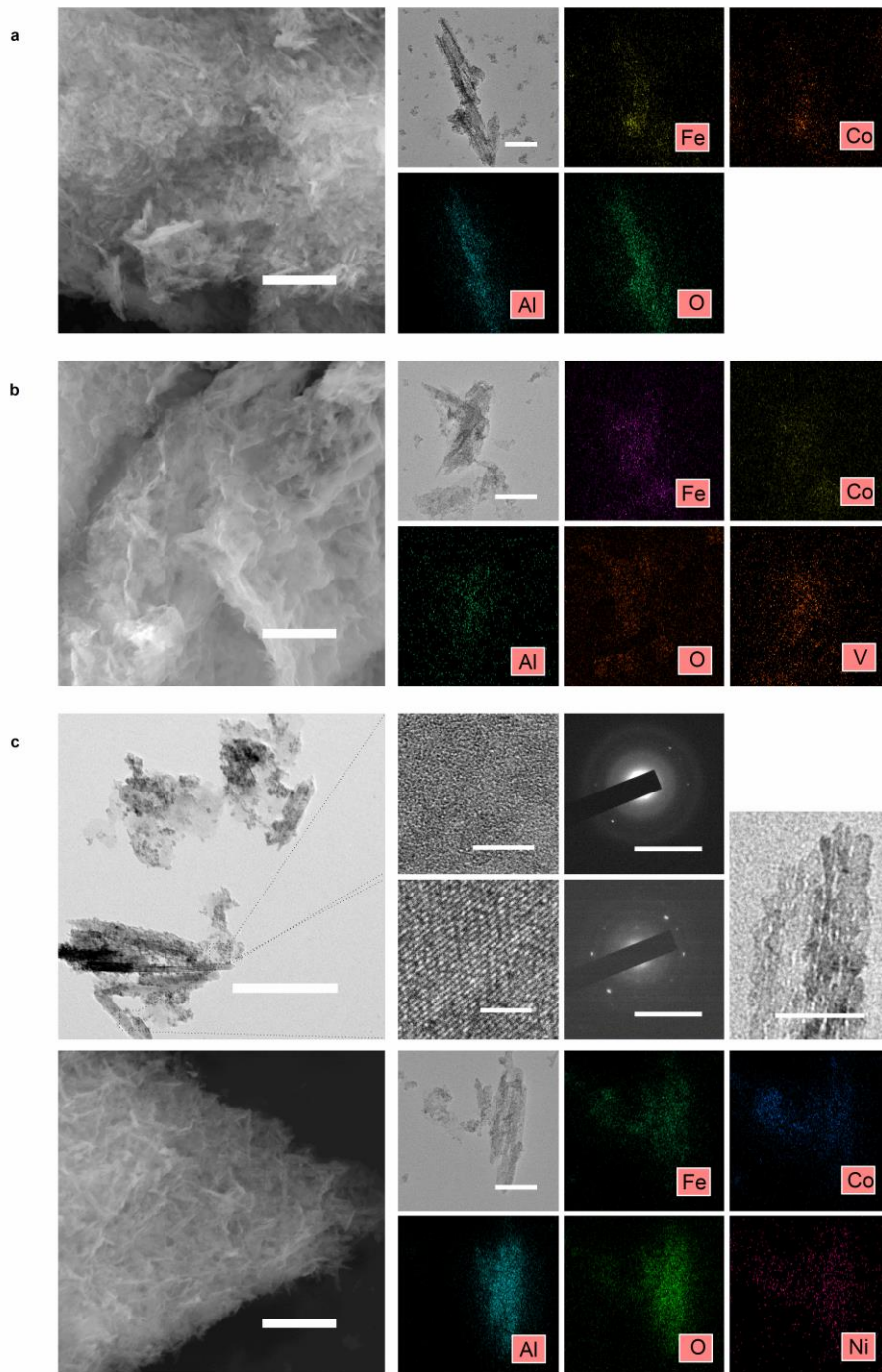


Fig. S11 Electron microscopy measurements of $\text{Fe}_1\text{Co}_1\text{-LDH}$ -based composites. FESEM images, TEM images and corresponding EDS mappings of a) AlOOH/FeCo-LDH , b) V-AlOOH/FeCo-LDH and c) Ni-AlOOH/FeCo-LDH . c) TEM image, HRTEM images and the corresponding SAED patterns, and the TEM image in a higher magnification of Ni-AlOOH/FeCo-LDH . Scale bar: $1\ \mu\text{m}$ for all the FESEM images, $100\ \text{nm}$ for the TEM image in a), $200\ \text{nm}$ for the TEM image in b) and c), $5\ \text{nm}$ and $2\ \text{nm}$ for the upper and downside HRTEM image in c), $10\ \text{nm}^{-1}$ for the SAED patterns, and $50\ \text{nm}$ for the higher-magnified TEM image.

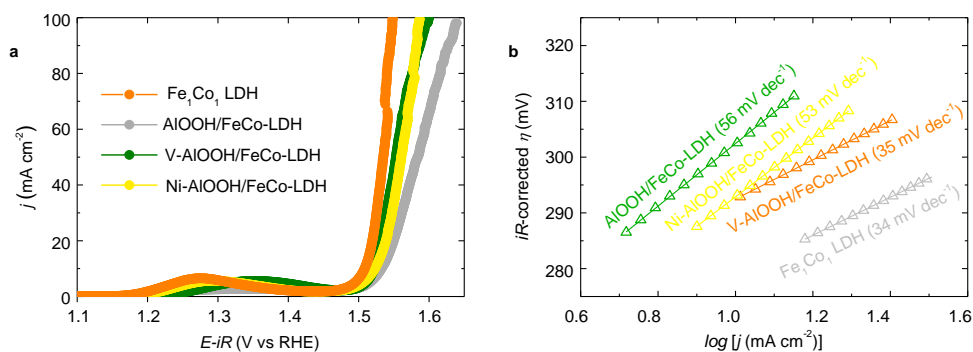


Fig. S12 Electrocatalytic properties of $\text{Fe}_1\text{Co}_1\text{-LDH}$ -based composites. a) LSV curves in O_2 -saturated 1 M KOH at 1600 rpm and b) the corresponding Tafel slopes of $\text{Fe}_1\text{Co}_1\text{-LDH}$ -based composites. Both of the overpotentials of Ni-AlOOH/FeCo-LDH and V-AlOOH/FeCo-LDH are 292 mV, a little smaller than that of AlOOH/FeCo-LDH, while the Tafel slope of V-AlOOH/FeCo-LDH is nearly the same as that of the pristine $\text{Fe}_1\text{Co}_1\text{ LDH}$, which is much smaller than those of other two composites.

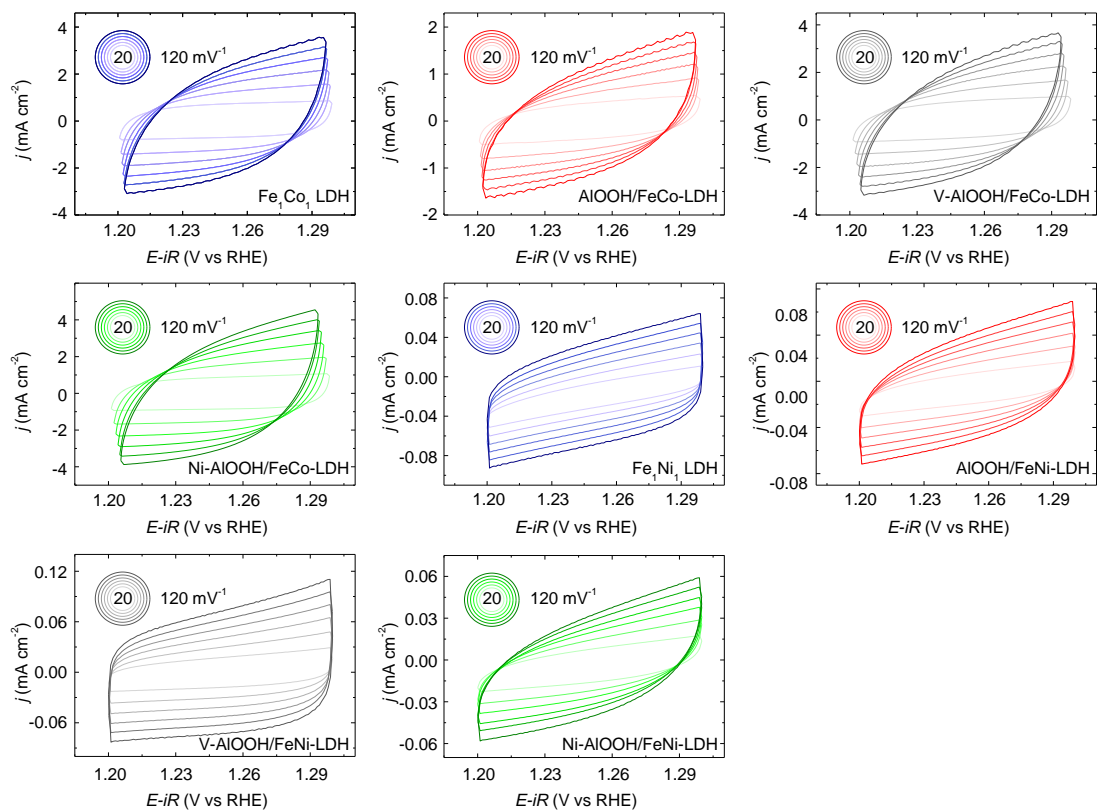


Fig. S13 Typical CV curves of these LDH-based composites with different scan rates varying from 20 to 120 mV s^{-1} in O_2 -saturated 1 M KOH at 1600 rpm.

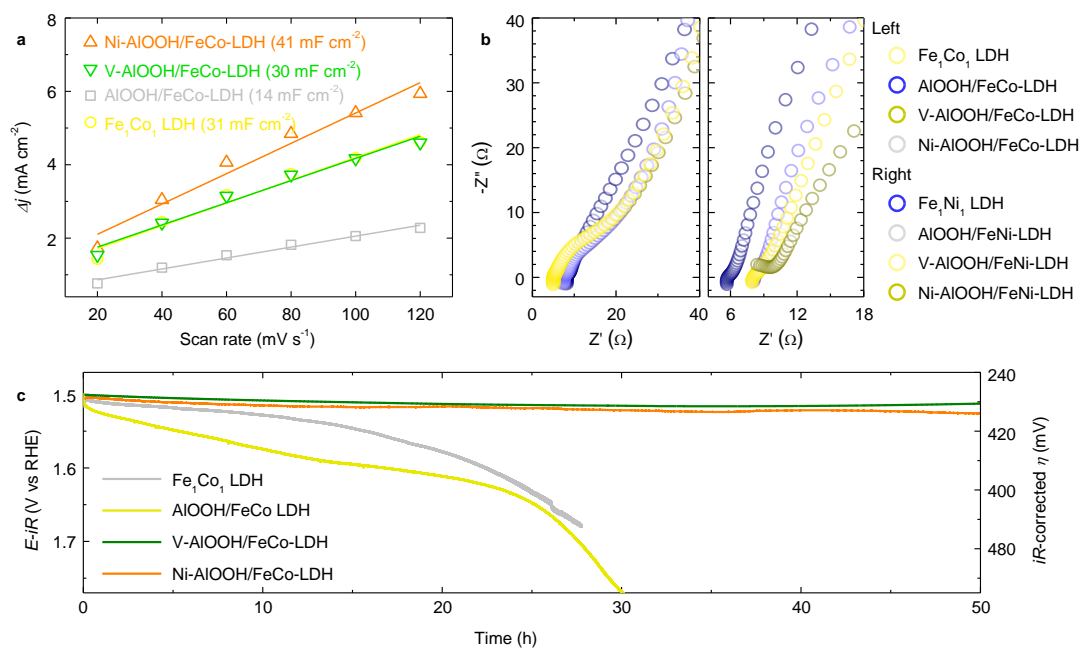


Fig. S14 Electrocatalytic properties of Fe_1Co_1 -LDH-based composites. a) ECSA plots and c) CP curves of Fe_1Co_1 -LDH-based composites. Comparing with Fe_1Ni_1 -LDH-based composites, both of V and Ni dopants seem quite efficient for the conduction of Fe and Co ions. The ECSAs of V-AIOOH/FeCo-LDH and the pristine Fe_1Co_1 LDH are nearly the same while AIOOH/FeCo-LDH obtains the smallest ECSA, demonstrating the important role of V and Ni dopants in AIOOH. b) Representative Nyquist plots of these composites.

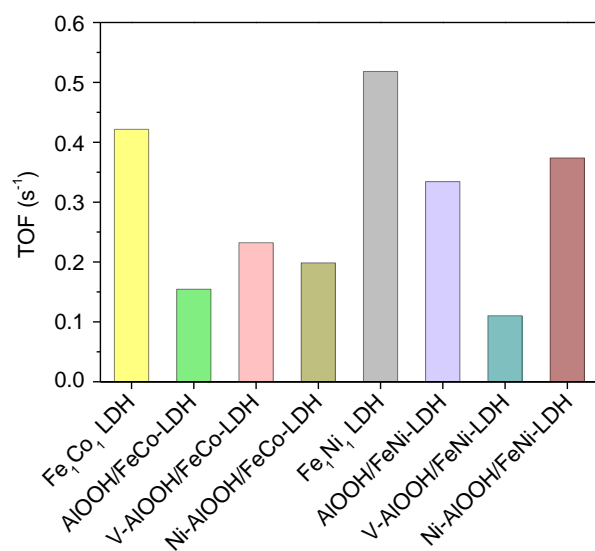


Fig. S15 TOFs of the composites calculated from the current at $\eta = 300$ mV.

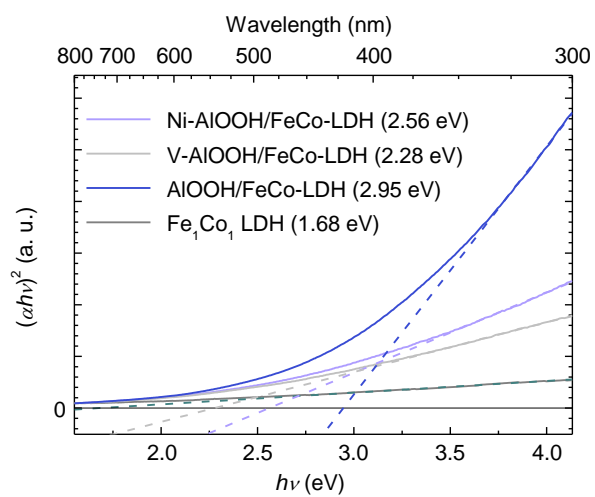


Fig. S16 Tauc plots of Fe₁Co₁-LDH-based composites.

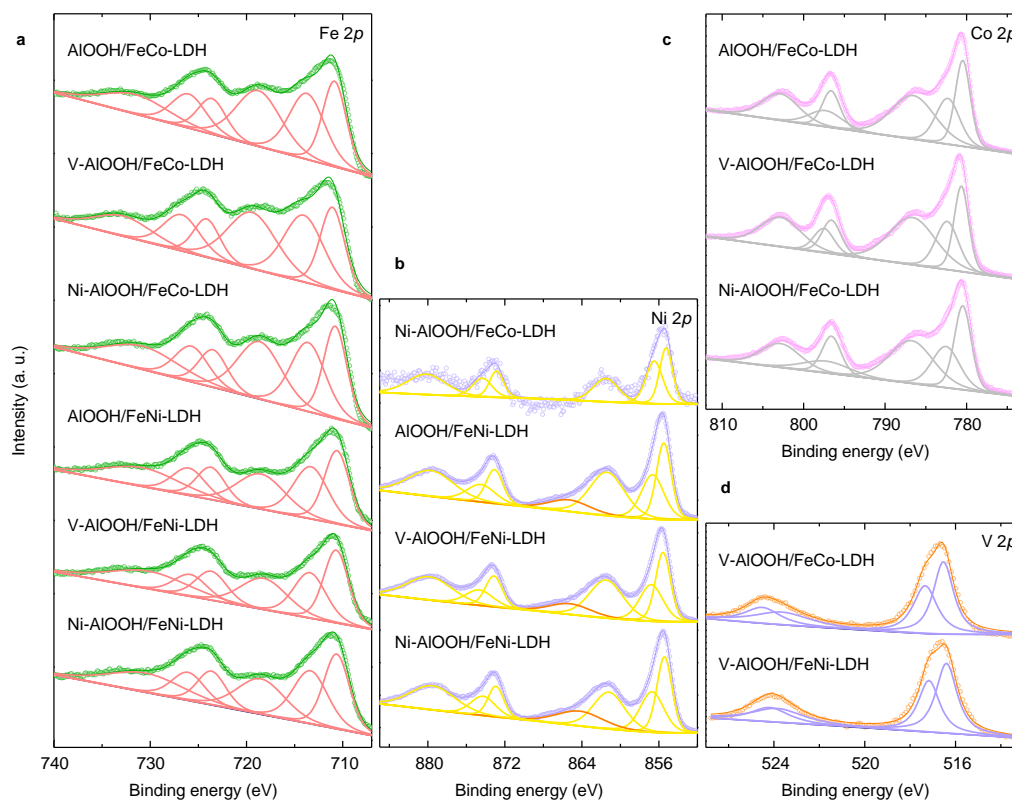


Fig. S17 a) Fe 2*p*, b) Ni 2*p*, c) Co 2*p* and d) V 2*p* XPS spectra for the composites. As the core levels of Fe 2*p* are generally tough, no obvious changes of Fe 2*p* for different composites could be observed, demonstrating stable chemical state, the same as Co 2*p* and V 2*p* XPS spectra.